Special Collection

Fine-Tuning the Photophysics of Donor-Acceptor (D-A$_3$) Thermally Activated Delayed Fluorescence Emitters Using Isomerisation

Paloma L. dos Santos,*[a, b] Daniel de Sa Pereira,[b] Julien Eng,[c] Jonathan S. Ward,[d] Martin R. Bryce,[d] Thomas J. Penfold,[c] and Andrew P. Monkman*[b]

Here two D–A$_3$ regioisomers, comprising three dibenzothiophene-S,S-dioxide acceptor units attached to a central triazatruxene core, are studied. Both molecules show thermally activated delayed fluorescence (TADF), however, the efficiency of the TADF mechanism is strongly affected by the D–A substitution position. The *meta-* substituted emitter (**1 b**) shows a slightly higher-lying singlet charge transfer state and a lower-lying triplet state than that observed in the *para-* substituted emitter (**1 a**), resulting in a larger singlet–triplet splitting (ΔE_{ST}) of 0.28 eV compared to only 0.01 eV found in **1 a**. As expected, this ΔE_{ST} difference strongly impacts the reverse intersystem crossing (rISC) rates and the *para-* isomer **1 a** exhibits a much faster delayed fluorescence emission. Calculations show that the triplet energy difference between the two isomers is due to steric hindrance variances along the donor–acceptor rotation axis in these molecules: as **1 b** is less restricted, rotation of its acceptor unit leads to a lower T$_1$ energy, further away from the region of high density of states (the region where larger vibronic coupling is found, favouring rISC). Therefore, our results show how the substitution pattern has a marked effect on triplet state energies and character, verifying the key structural designs for highly efficient TADF materials.

Introduction

Research into novel high-performing emitters for organic light emitting diodes (OLEDs)[1] has gathered great interest in the scientific and industrial communities alike, particularly with its third generation, where devices based on thermally activated delayed fluorescence (TADF) emitters have been extensively produced and optimised. TADF emitters are particularly appealing as they can achieve 100% internal quantum efficiency (IQE),

while retaining the use of purely organic molecules. In these materials the non-emissive triplet excitons are converted into emissive singlet excitons via reverse intersystem crossing (rISC).[2,3] The potential of achieving highly efficient purely organic emitters in OLEDs has been the driving force behind a significant research effort aimed at achieving a deep understanding of efficient molecular design strategies that can avoid the production of materials that show emission loss pathways that will reduce device performance.[4,5]

The most common molecular design strategy to achieve efficient TADF emitters is to use aromatic donor–acceptor (D–A) molecules, which typically have near-orthogonal separation between the D and A units, decoupling the conjugation between them. These molecules emit from a singlet excited state with intramolecular charge transfer (^{1}CT) character, which is energetically very close to a ^{3}CT triplet state through the minimised electron exchange interaction. A further excited state with dissimilar orbital symmetry such as a local excited triplet state (^{3}LE) situated very close in energy to this ^{1}CT is also required for efficient triplet harvesting via reverse intersystem crossing (rISC).[6,7] The current D–A TADF molecules still face the challenge of the long overall delayed fluorescence lifetimes (which in turn will adversely affect the device lifetime) and the low oscillator strengths of the ^{1}CT radiative transitions. We have recently shown a novel design strategy based on a rigid donor unit (D, triazatruxene) and three acceptor units (A, dibenzothiophene-S,S-dioxide), which results in fast rISC rates (10^7 s^{-1}).[8] This D–A$_3$ emitter, previously named TAT-3DBTO$_2$ (here renamed as **1 a**; Figure 1a), shows excellent device performance, presenting a new design strategy very promising for high performing OLEDs, which was proposed to arise from the high density of coupled excited states.[9] Other workers have

[a] Dr. P. L. dos Santos
Department of Engineering
Durham University
DH1 3LE Durham, (UK)
E-mail: paloma.l.dos-santos@durham.ac.uk

[b] Dr. P. L. dos Santos, Dr. D. de Sa Pereira, Prof. A. P. Monkman
Department of Physics
Durham University
DH1 3LE Durham, (UK)
E-mail: paloma.l.dos-santos@durham.ac.uk
a.p.monkman@durham.ac.uk

[c] Dr. J. Eng, Prof. T. J. Penfold
Chemistry School of Natural and Environmental Sciences
Newcastle University
NE1 7RU Newcastle, (UK)

[d] Dr. J. S. Ward, Prof. M. R. Bryce
Department of Chemistry
Durham University
DH1 3LE Durham, (UK)

Special Collection An invited contribution to a Special Collection on Emissive Materials for Organic Light Emitting Diodes.
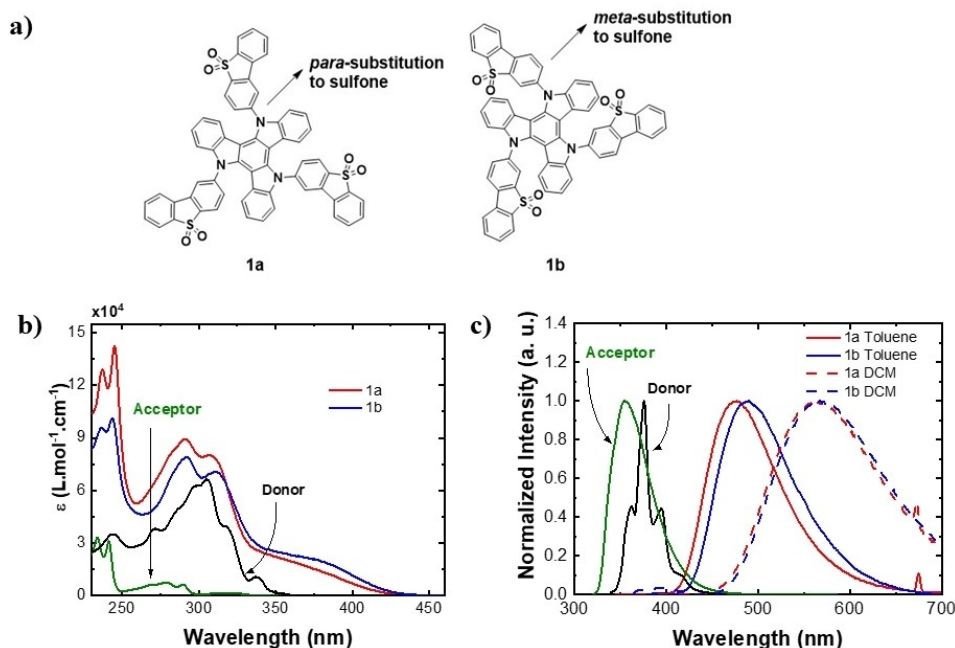
Figure 1. a) Chemical structure of *para*- substituted emitter (**1a**) and *meta*- substituted emitter (**1b**). b) Extinction coefficient absorption spectra of the acceptor (A), donor (D), **1a** and **1b**, all diluted in dichloromethane (DCM) solvent. c) Normalised photoluminescence (PL) spectra of A, D, **1a** and **1b**. D and A are diluted in toluene solvent, **1a** and **1b** are diluted in toluene and DCM. Data for A, D and **1a** are taken from Reference [8].

subsequently studied TADF emitters containing triazatruxene in D–A₂,[10] D–A,[11] D₂–A[12,13] and D₃–A structures[14] demonstrating the versatility of triazatruxene in this context.

To further investigate the D–A₃ design strategy, herein we study the role of regioisomerisation on the emission by exploring how the substitution position of the sulfone group of the A units in the *meta-* and *para-* positions relative to the N atoms of the donor affects the TADF mechanism. We provide extended photophysics of *para*-compound (**1a**) together with the characterisation of the novel isomeric *meta*-compound (**1b**). We show that the energy splitting between singlet and triplet states and consequently, the delayed fluorescence lifetime and reverse intersystem crossing (rISC) rates are strongly affected by the D–A substitution position, even though their molecular orientation is only slightly changed. **1b** has triplet excited states acting as traps, resulting in excitons with long overall residence times in the triplet excited states at much lower energy than **1a**, greatly increasing the delayed fluorescence (DF) lifetime. Calculations at the T₁ minimum geometry show that the triplet states of **1a** and **1b** have different energies and characters (purely LE or mixed CT/LE). These differences are due to the difference in steric hindrance along the donor–acceptor rotation axis that results in a stabilisation of **1b** at a lower energy minimum of T₁. Moreover, the calculations show that the lack of a close-lying electronic state in **1b** is critical in preventing efficient rISC in this molecule. Thus, our experimental and theoretical results show how subtle changes in a D–A₃ structure radically effect the excited state behaviour and photophysical properties.

Results and Discussion

Figure 1a shows the chemical structure of the two isomers, **1a** (*para*-substitution) and **1b** (*meta*-substitution). Figure 1b shows the extinction coefficient absorption spectra of both emitters together with the individual D and A units, all measured in dichloromethane (DCM) solutions. Both molecules show similar spectra, as expected by the similarity of both emitters in the ground state geometry, in line with their respective calculations (SI1

5). There is a general enhancement of extinction coefficient at all wavelengths in both isomers, compared to the individual D and A units. The absorption band at lower energy (350 nm to 425 nm), which is not observed in the individual D or A units, is ascribed to direct CT absorption to the CT excited states. Excitation into this band which directly populates ¹CT excited states is more intense in **1b** as well as being red shifted compared to **1a** indicating a more delocalised state in **1b**.

Figure 1c shows the photoluminescence (PL) spectra of **1a** and **1b** in toluene and DCM. The spectra are clearly indicative of CT emission, displaying a Gaussian band shape and strong positive solvatochromism. In toluene, **1b** shows emission slightly red shifted compared to **1a**, in agreement with its red shifted absorption band. This feature agrees with the calculations, which show that in the geometry of the minimum of S₁, **1b** features one acceptor closer to orthogonality than in **1a** (the D–A torsion angle φ : φ(**1a**)=77.49 deg, φ(**1b**)= 79.70 deg). This leads to a smaller highest occupied/lowest unoccupied molecular orbital (HOMO/LUMO) overlap at S₁ minimum: S(**1a**)=14.33%, S(**1b**)=11.38%, resulting in an increased CT character for **1b**. However, in DCM the emission

from both isomers converges to the same energy indicating a saturation of the CT stabilisation, which is therefore independent of the *para-* and *meta-* substitution between D and A units.[4]

We next investigated both emitters in an inert solid-state matrix, zeonex. In both cases, the films were produced in very low emitter concentration (0.3% wt), as strong aggregation was observed when the concentration was increased (See SI1). Interestingly, the PL emission observed in **1b** is at higher energy than **1a** (Figure 2a), contrary of the results observed in toluene solution (Figure 1c). Zeonex is a non-polar environment, but emission from **1b** occurs at the same energy as observed in toluene, whereas **1a** is red shifted to an energy below that found in toluene. This indicates that packing forces from the zeonex host influence the orientation of D and A but to different degrees for the two isomers. In both cases the CT states are stabilised by the host via packing interactions but **1a** is more strongly stabilised, potentially indicating greater potential CT character in the **1a** excited states. However, **1b** shows broader emission, indicating greater disorder and possible higher number of emissive states contributing to the overall emission band (sum of Gaussian).[15]

To investigate how the TADF mechanism is affected in both emitters, the emission decay curves at room temperature (RT) were measured (Figure 2b). Initially, rather slow prompt fluorescence (PF) is observed up to 230 ns followed by a longer-lived emission – delayed fluorescence (DF). The DF emission observed in **1a** clearly shows two distinct regions, a fast decay – between 230 ns and 6 μs and a long-lived tail up to 250 μs. On the other hand, **1b** shows a single delayed decay

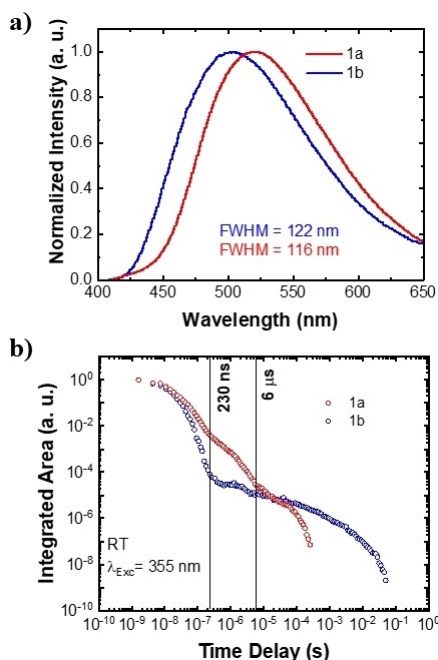feature following PF emission, which is much longer lived than the DF observed in **1a**, and extends up to the *ms* region. It is important to note that for efficient total emission, TADF emitters do not require to show high contribution of DF emission if they show high yield of PF emission, low ISC and unity rISC yields.[8] This will result in the majority of excitons formed in the singlet states to emit via PF and just a small population of excitons to be converted back to triplet states. This is observed in both emitters, as the contribution of DF to the overall emission, which was analysed by using the area under the PF and DF regions, represents a small parcel of the total emission, 10% and 30% for **1a** and **1b** molecules, respectively.

Figure 3 shows the spectra collected at different time delays (TD). Both emitters show strong relaxation in the first 100 ns (Figure 3a, e) which is associated with the energetic relaxation of the CT state. The value of the onset energy of the spectrum collected at TD = 1.6 ns and TD = 105 ns is shown in the graphs. The relaxation observed in the first 100 ns is similar for both emitters, 0.10 eV and 0.8 eV, respectively, for **1a** and **1b**. The prompt emission observed in **1b** is at higher energies than **1a**, in line with the steady state results (Figure 2a). Between 230 ns and 6 μs, little spectral change is observed. After 6 μs, the red edge of the DF spectra emits faster in **1a**. For **1b**, a clear blue shift is observed with increasing time delays, again pointing to emission at longer wavelength showing faster emission. Such spectral dynamics were discussed by Penfold *et al*[15] and arise from a dispersion of rISC rates that stem from a variety of subtly different molecular conformations (of D with respect to A). The conformers that have a higher ^{1}CT energy and oscillator strength have a larger energy splitting between singlet and triplet states (ΔE_{ST}), which will slow down the rISC, due to its exponential dependence on the energy gap. Therefore, conformations with smaller ΔE_{ST} will emit first in the DF region, leading to the later emission exhibiting a blue shift. This dynamic component, which is clearly more pronounced in **1b** compared to **1a**, broadens the steady state emission spectrum and likely the electroluminescence spectra of devices, which is undesirable for the colour purity of the devices.

Measurements at 80 K in zeonex matrix, show a much-reduced TADF intensity, compared to RT, with phosphorescence (PH) being observed at longer times at 80 K in both compounds (See SI2 spectra from the decay curves of Figure 4a). **1a** has been investigated in our previous work in bis-4-(*N*-carbazolyl)phenyl)phenylphosphine oxide (BCPO)[16] host at 80 K, and contrary to what is seen here, TADF emission was observed even at 80 K in BCPO indicating rISC was active even with very little thermal energy available.[8] Figure 4b shows their PH spectra in a zeonex matrix, collected on the millisecond timescale and at low temperature (80 K). Both PH spectra are well structured showing a marked ^{3}LE character, onset at 2.62 eV for **1b** and 2.77 eV for **1a**. Moreover, **1a** PH spectra were investigated in different hosts and shown to be almost unaffected by the host dielectric environment (see SI3), which is also a typical characteristic of a LE character. Interestingly, a red shift is observed between the onset of the PH spectrum of **1a** and **1b**, opposite to the blue shift observed in the singlet
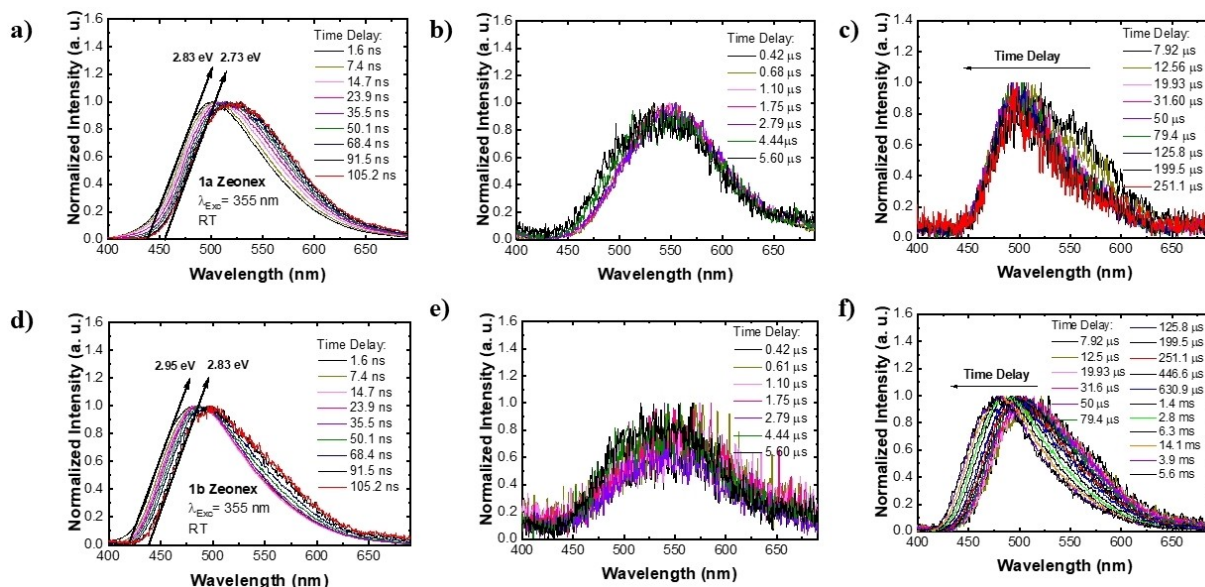

Figure 2. a) Normalised photoluminescence (PL) spectra of **1a** and **1b** in zeonex matrix; FWHM is full width at half maximum. b) Normalised decay curves of **1a** and **1b** in zeonex matrix collected at room temperature under vacuum.

ChemPhotoChem

Research Articles
doi.org/10.1002/cptc.202200248

Chemistry Europe
European Chemical
Societies Publishing

Figure 3. a, b, c) Time resolved normalised emission spectra of **1a** and d, e, f) **1b** in zeonex matrix. All spectra collected at room temperature under vacuum.
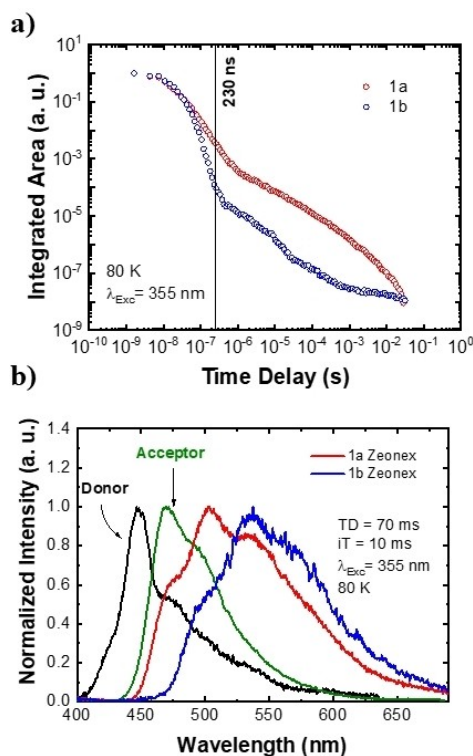

Figure 4. a) Normalised decay curves of **1a** and **1b** in zeonex matrix collected at 80 K under nitrogen atmosphere. B) Normalised phosphorescence (PH) of acceptor (A), donor (D), **1a** and **1b** molecules, all in zeonex matrix collected at 80 K.

states (Figure 1c), which translates into a very different energy splitting between singlet and triplet ($\triangle E_{ST}$) in both emitters. The $\triangle E_{ST}$ was estimated to be 0.28 eV and 0.01 eV for **1b** and **1a**, respectively (SeeSI4). The large $\triangle E_{ST}$ observed in **1b** film explains why this emitter shows long lived delayed

fluorescence at room temperature when compared to **1a** film, as $\triangle E_{ST}$ and DF lifetime are proportional to each other.[17]

Importantly, the calculations at the T_1 minimum geometry show that for **1b** T_1 has a mixed $^3CT/^3LE(A)$ character. On the other hand, for **1a**, T_1 is of pure $^3LE(A)$ character. This is due to the more important steric hindrance along the donor–acceptor rotation in **1a** than in **1b**. While the local excitation on the acceptor is not affected by the torsion, in **1b** the acceptor unit can rotate further to lower the charge transfer energy and decrease the energy gap with the lower lying $^3LE(A)$. This energy gap becomes so small that the vibronic coupling between T_1 and T_2 leads to a stabilisation of the former explaining the lower energy minimum of T_1 in **1b** than in **1a**.

Figure 5 shows a schematic representation of the evolution of the singlet and triplet charge transfer states and a local excitation on the acceptor unit as a function of the torsion angle around the donor–acceptor bond. As **1b** is less restricted by steric hindrance, rotation of the acceptor unit leads to a lower T_1 energy, further away from the region of high density of states. As Eng *et al.* have previously shown,[9] this leads to a slower reverse intersystem crossing rate and therefore a slower DF lifetime of **1b** in comparison to **1a**. Similarly, the stabilisation of the singlet ^1CT states is greater in **1b** than in **1a** further decreasing the density of states. While the energy gap between ^1CT and ^3CT in **1b** is smaller, the TADF efficiency is reduced as the system lacks a close-lying electronic state to mediate rISC.

Moreover, we investigated the PH emission spectra when CT states are directly excited via 420 nm excitation, Figure 6. For **1a**, the PH spectrum is located at lower energies if compared to the PH spectrum observed when the LE states are excited (at 266 nm or 355 nm). However, for **1b**, the energy of PH spectra does not depend as strongly on the excitation energy. We speculate that this difference of behaviour might be explained by a local minimum in the lowest T_1 states that is

ChemPhotoChem

Research Articles
doi.org/10.1002/cptc.202200248

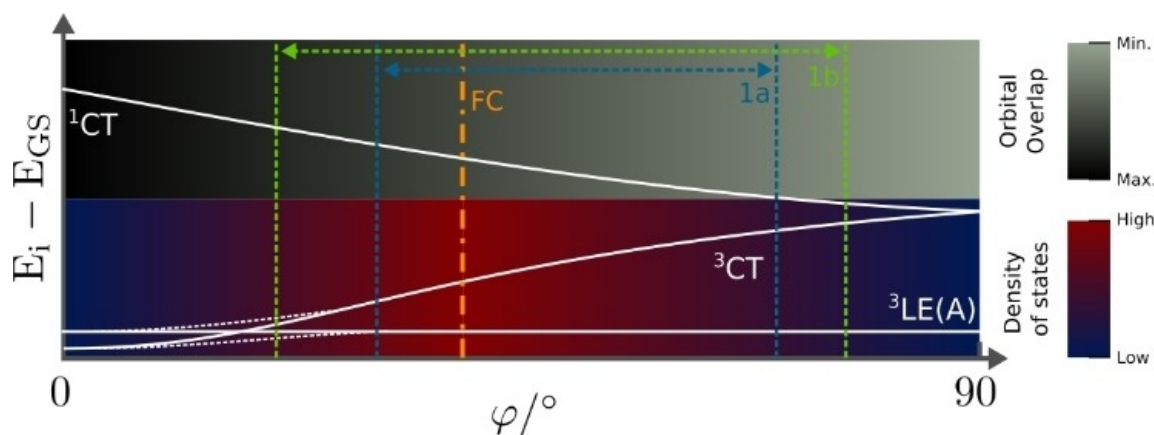**Chemistry Europe**
European Chemical
Societies Publishing

Figure 5. Schematic representation on the evolution of the energy of CT and LE states as a function of the torsion around the donor–acceptor bond (ϕ). The orbital overlap as well as the density of states are given under the form of colour gradients. Full white lines represent the excitation energy of "pure" diabatic states. Dashed lines represent adiabatic states resulting from the non-adiabatic coupling occurring between diabatic states. The dashed orange line represents the Franck-Condon region and the dashed blue and green lines represent the region of space accessible by **1a** and **1b**, respectively.
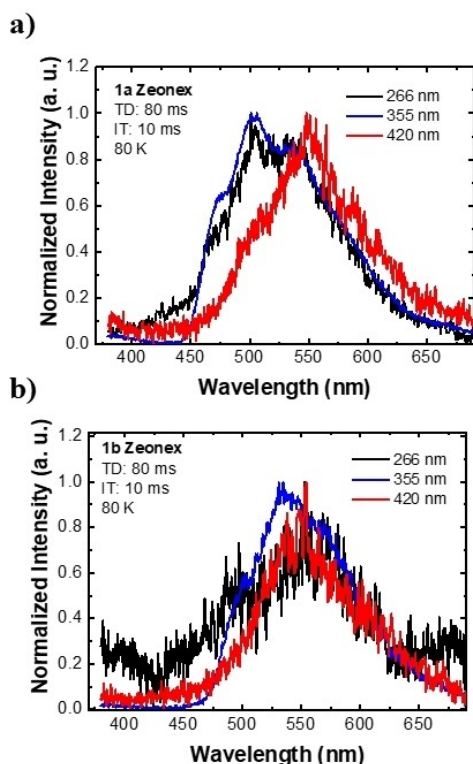

Figure 6. Normalised phosphorescence (PH) of a) **1a** and b) **1b**, all in zeonex matrix collected at 80 K, varying the excitation wavelength.

accessible in **1a** (such a minimum could not be identified in the theoretical calculations) and not in **1b**. The time evolution of the **1a** PH with 355 nm excitation, (Figure SI3a) shows an initial low energy CT like emission at 1 ms which evolves into well-structured higher energy PH by 80 ms. Whereas in **1b** there is much less spectral evolution in time (Figure SI3b), with less structured PH at 80 ms. This evolution could be driven by excess excitation energy and thus at lower excitation energy (420 nm) there is not enough excess energy to drive the triplet state to the higher fully localised state present in **1a**, whereas in **1b** this channel is not available.

Conclusion

In summary, we report the photophysical properties in solutions and solid state as well as theoretical calculations of two D–A₃ regioisomers, named **1a** (*para*-compound) and **1b** (*meta*-compound). We identified strong aggregation formation of **1a** in solid state even at only 1.5% wt in zeonex matrix, impacting the energy and spectral shape of its singlet and triplet states. Thus, photophysical characterisation was performed for both materials at very low concentration, 0.3% wt in zeonex matrix. The TADF mechanism was readily identified for both compounds (**1a** $\Delta E_{ST} = 0.01$ eV and **1b** $\Delta E_{ST} = 0.28$ eV), however their efficiency is strongly affected by the D–A substitution position. The major difference between both isomers is related to their triplet state energies (**1a** $T_1 = 2.77$ eV and **1b** $T_1 = 2.62$ eV). Calculations show that this energy difference is due to steric hindrance variances along the donor–acceptor rotation axis in these molecules: as **1b** is less restricted, rotation of its acceptor unit leads to a lower T_1 energy, further away from the region of high density of states. Moreover, **1a** shows much faster delayed fluorescence than that observed in **1b**, a direct result from its lower ΔE_{ST} found experimentally as well as its T_1 being closer to the region where larger vibronic coupling is found, as revealed by the calculations. Thus, our results represent an important step forward in the clear understanding of how the substitution pattern has a marked effect in achieving enhanced TADF.

Experimental Section

The synthesis and characterisation of **1b** are presented in the Supporting Information.

ChemPhotoChem

Research Articles
doi.org/10.1002/cptc.202200248

**Chemistry
Europe**
European Chemical
Societies Publishing

Solutions of **1a** and **1b** were studied (10^{-3} to 10^{-5} M) in toluene and dichloromethane (DCM). All the solutions were stirred for several hours to ensure complete dissolution. **1a** and **1b** spin coating films were produced in zeonex matrix at a concentration of 0.3 % wt. The films were dispersed onto quartz substrates.

Steady state absorption and emission spectra were acquired using a UV-3600 Shimadzu spectrophotometer and a Jobin Yvon Horiba Fluoromax 3, respectively. Time resolved spectra were obtained by exciting the sample with a Nd:YAG laser (EKSPLA), 10 Hz, 355 nm. Sample emission was directed onto a spectrograph and gated iCCD camera (Stanford Computer Optics). Time resolved measurements were carried out at room temperature with zeonex films under vacuum and at 80 K with films under nitrogen gas.

Computational Details

All the calculations were performed using the Qchem 5.0 quantum chemistry package.[18] **1a** and **1b** were optimised in the ground and lowest singlet and triplet excited states using density functional theory (DFT) and linear response time-dependent DFT (LR-TDDFT), respectively.

Vibrational analysis was performed to ensure all frequencies were positive and that the stationary point was a minimum of the potential energy surface. All calculations were performed with the 6-31G* Pople basis set[19–21] and the range-corrected LRC-ωPBEh functional.[22] The range separation parameter ω was optimised using the optimal tuning method as described here[23–26] and the optimal value obtained was $\omega = 0.131 a_0^{-1}$. The Tamm-Dancoff approximation[27] has been employed to avoid the overstabilisation of the low-lying intra-ligand triplet states.

The data that support the findings of this study are openly available in Open Data Commons Open Database License under DOI: 10.25405/data.ncl.20488341.v1.

Author contributions

PLdS and DdSP performed all steady state and time resolved photophysical characterization under supervision of APM. JE performed calculations under the supervision of TJP. JSW designed the molecules and performed the synthesis, purification and characterisation under the supervision of MRB. All authors contributed to the manuscript writing.

Conflict of Interest

The authors declare no conflict of interest.

Data Availability Statement

The data that support the findings of this study are available from the corresponding author upon reasonable request.

[1] C. W. Tang, S. A. VanSlyke, *Appl. Phys. Lett.* **1987**, *51*, 913.
[2] H. Uoyama, K. Goushi, K. Shizu, H. Nomura, C. Adachi, *Nature* **2012**, *492*, 234.
[3] P. L. dos Santos, M. K. Etherington, A. P. Monkman, *J. Mater. Chem. C* **2018**, *6*, 4842.
[4] C. S. Oh, D. d. S. Pereira, S. H. Han, H. J. Park, H. F. Higginbotham, A. P. Monkman, J. Y. Lee, *ACS Appl. Mater. Interfaces* **2018**, *10*, 35420.
[5] Y. Im, M. Kim, Y. J. Cho, J.-A. Seo, K. S. Yook, J. Y. Lee, *Chem. Mater.* **2017**, *29*, 1946.
[6] J. Gibson, A. Monkman, T. Penfold, *ChemPhysChem* **2016**, *17*, 2956.
[7] J. Gibson, T. J. Penfold, *Phys. Chem. Chem. Phys.* **2017**, *19*, 8428.
[8] P. L. dos Santos, J. S. Ward, D. G. Congrave, A. S. Batsanov, J. Eng, J. E. Stacey, T. J. Penfold, A. P. Monkman, M. R. Bryce, *Adv. Sci.* **2018**, *5*, 1700989.
[9] J. Eng, J. Hagon, T. J. Penfold, *J. Mater. Chem. C* **2019**, *7*, 12942.
[10] Y. Liu, X. Wu, Y. Chen, L. Chen, H. Li, W. Wang, S. Wang, H. Tian, H. Tong, L. Wang, *J. Mater. Chem. C* **2019**, *7*, 9719.
[11] Y. Liu, B. Du, X. Han, X. Wu, H. Tong, L. Wang, *Chem. Eng. J.* **2022**, *446*, 137372.
[12] Y. Chen, S. Wang, X. Wu, Y. Xu, H. Li, Y. Liu, H. Tong, L. Wang, *J. Mater. Chem. C* **2018**, *6*, 12503.
[13] Y. Liu, Y. Chen, H. Li, S. Wang, X. Wu, H. Tong, L. Wang, *ACS Appl. Mater. Interfaces* **2020**, *12*, 30652.
[14] S. K. Pathak, H. Liu, C. Zhou, G. Xie, C. Yang, *J. Mater. Chem. C* **2021**, *9*, 7363.
[15] T. Northey, J. Stacey, T. J. Penfold, *J. Mater. Chem. C* **2017**, *5*, 11001.
[16] H.-H. Chou, C.-H. Cheng, *Adv. Mater.* **2010**, *22*, 2468.
[17] T. Palmeira, M. N. Berberan-Santos, *J. Phys. Chem. C* **2017**, *121*, 701.
[18] Y. Shao, Z. Gan, E. Epifanovsky, A. T. B. Gilbert, M. Wormit, J. Kussmann, A. W. Lange, A. Behn, J. Deng, X. Feng, D. Ghosh, M. Goldey, P. R. Horn, L. D. Jacobson, I. Kaliman, R. Z. Khaliullin, T. Kuś, A. Landau, J. Liu, E. I. Proynov, Y. M. Rhee, R. M. Richard, M. A. Rohrdanz, R. P. Steele, E. J. Sundstrom, H. L. Woodcock, P. M. Zimmerman, D. Zuev, B. Albrecht, E. Alguire, B. Austin, G. J. O. Beran, Y. A. Bernard, E. Berquist, K. Brandhorst, K. B. Bravaya, S. T. Brown, D. Casanova, C.-M. Chang, Y. Chen, S. H. Chien, K. D. Closser, D. L. Crittenden, M. Diedenhofen, R. A. DiStasio, H. Do, A. D. Dutoi, R. G. Edgar, S. Fatehi, F. Fusti-Molnar, A. Ghysels, A. Golubeva-Zadorozhnaya, J. Gomes, M. W. D. Hanson-Heine, P. H. P. Harbach, A. W. Hauser, E. G. Hohenstein, Z. C. Holden, T.-C. Jagau, H. Ji, B. Kaduk, K. Khistyaev, J. Kim, J. Kim, R. A. King, P. Klunzinger, D. Kosenkov, T. Kowalczyk, C. M. Krauter, K. U. Lao, A. D. Laurent, K. v. Lawler, S. v. Levchenko, C. Y. Lin, F. Liu, E. Livshits, R. C. Lochan, A. Luenser, P. Manohar, S. F. Manzer, S.-P. Mao, N. Mardirossian, A. v. Marenich, S. A. Maurer, N. J. Mayhall, E. Neuscamman, C. M. Oana, R. Olivares-Amaya, D. P. O'Neill, J. A. Parkhill, T. M. Perrine, R. Peverati, A. Prociuk, D. R. Rehn, E. Rosta, N. J. Russ, S. M. Sharada, S. Sharma, D. W. Small, A. Sodt, T. Stein, D. Stück, Y.-C. Su, A. J. W. Thom, T. Tsuchimochi, V. Vanovschi, L. Vogt, O. Vydrov, T. Wang, M. A. Watson, J. Wenzel, A. White, C. F. Williams, J. Yang, S. Yeganeh, S. R. Yost, Z.-Q. You, I. Y. Zhang, X. Zhang, Y. Zhao, B. R. Brooks, G. K. L. Chan, D. M. Chipman, C. J. Cramer, W. A. Goddard, M. S. Gordon, W. J. Hehre, A. Klamt, H. F. Schaefer, M. W. Schmidt, C. D. Sherrill, D. G. Truhlar, A. Warshel, X. Xu, A. Aspuru-Guzik, R. Baer, A. T. Bell, N. A. Besley, J.-D. Chai, A. Dreuw, B. D. Dunietz, T. R. Furlani, S. R. Gwaltney, C.-P. Hsu, Y. Jung, J. Kong, D. S. Lambrecht, W. Liang, C. Ochsenfeld, V. A. Rassolov, L. v. Slipchen-

ChemPhotoChem

Research Articles
doi.org/10.1002/cptc.202200248

Chemistry Europe
European Chemical
Societies Publishing

ko, J. E. Subotnik, T. van Voorhis, J. M. Herbert, A. I. Krylov, P. M. W. Gill, M. Head-Gordon, *Mol. Phys.* **2015**, *113*, 184.

[19] R. Ditchfield, W. J. Hehre, J. A. Pople, *J. Chem. Phys.* **1971**, *54*, 724.

[20] W. J. Hehre, R. Ditchfield, J. A. Pople, *J. Chem. Phys.* **1972**, *56*, 2257.

[21] P. C. Hariharan, J. A. Pople, *Mol. Phys.* **1974**, *27*, 209.

[22] M. A. Rohrdanz, K. M. Martins, J. M. Herbert, *J. Chem. Phys.* **2009**, *130*, 054112.

[23] T. J. Penfold, *J. Phys. Chem. C* **2015**, *119*, 13535.

[24] E. Livshits, R. Baer, *Chem. Phys.* **2007**, *9*, 2932.

[25] H. Sun, C. Zhong, J.-L. Brédas, *J. Chem. Theory Comput.* **2015**, *11*, 3851.

[26] J. Eng, B. A. Laidlaw, T. J. Penfold, *J. Comput. Chem.* **2019**, *40*, 25868.

[27] S. Hirata, M. Head-Gordon, *Chem. Phys. Lett.* **1999**, *314*, 291.